

Transition in Splitting Probabilities of Quantum Walks

Prashant Singh,^{1,*} David A. Kessler,¹ and Eli Barkai^{1,2}

¹*Department of Physics, Bar-Ilan University, Ramat Gan 52900, Israel*

²*Institute of Nanotechnology and Advanced Materials, Bar-Ilan University, Ramat Gan 52900, Israel*

We investigate the splitting probability of a monitored continuous-time quantum walk with two targets and show that, in stark contrast to a classical random walk, it exhibits a nonanalytic, phase-transition-like behavior controlled by the sampling time at the targets. For large systems and sampling times smaller than a critical value $\tau_c = 2\pi/\Delta E$, where ΔE is the energy bandwidth, the splitting probability is universal and equal to $1/2$, independent of the initial condition and the sampling time. Above the critical sampling, a nonuniversal regime emerges in which the splitting probability deviates from $1/2$ and develops a fluctuating pattern of pronounced peaks and dips dependent on both the sampling time and the initial condition. These results follow from a nontrivial mapping of the splitting problem onto a pair of single-target detection problems enabled by the superposition principle.

Introduction: Imagine a gambler entering a fair game with a finite initial fortune and aiming to win a predetermined amount, which defines success. At each bet, they gain or lose a part of their current fortune with equal probability. Chance governs every move, yet fate is unavoidable: the gambler either wins or goes bankrupt [1]. What is the probability that they end up winning rather than losing? This question lies at the heart of the *gambler's ruin problem*, where one seeks the splitting probability of achieving one outcome before the other.

The formulation admits a natural interpretation in terms of a one-dimensional unbiased random walk moving along a finite lattice with N number of sites and initial position x_0 (with $x_0 \in \{1, 2, \dots, N\}$) [2–4]. The left and right edges of the lattice, $x_L = 1$ and $x_R = N$, act as absorbing boundaries so that the walker is absorbed once it reaches a boundary and the process stops. Eventually, two outcomes are possible: the walker is absorbed at either the left or the right boundary, analogous to winning or losing in the gambler's ruin problem.

The splitting probabilities, $P_L^{(\text{cl})}(x_0)$ and $P_R^{(\text{cl})}(x_0)$, to the left and the right boundaries are [3]

$$P_L^{(\text{cl})}(x_0) = \frac{(N - x_0)}{(N - 1)}, \quad P_R^{(\text{cl})}(x_0) = 1 - P_L^{(\text{cl})}(x_0), \quad (1)$$

where “cl” denotes the classical nature of the process. The probabilities depend linearly on the initial position. Moreover, the classical walker obeys the proximity effect: the closer the walker starts to a boundary, the more likely it is to be absorbed there. The splitting-probability framework has found wide applications in biophysical systems [5–7], stochastic thermodynamics [8], polymer physics [9], stochastic transport processes [10–13] and restarted processes [14–16].

Plurality of possible outcomes can also have far-reaching implications in quantum settings, motivated by the expanding scope of quantum applications. For exam-

ple, in quantum communication, spin-chain-based quantum wires are explicitly used to transmit information from one end of the wire to the other [17–20]. The performance of the wire is directly related to how well the signal reaches the intended end rather than being reflected back. Similarly, in quantum walk-based algorithms, one often involves search processes featuring many targets, and it is highly desirable to optimize the performance to locate these various targets efficiently [21–25]. Likewise, in quantum circuits, the performance depends on whether gate operations can be successfully completed before qubits are irreversibly lost due to noise in the circuit [26].

At a fundamental level, such considerations naturally lead to quantum walks with two absorbing boundaries, which provide a minimal setting for analyzing competing outcomes. In an early work, Ambainis et al. analyzed discrete-time Hadamard quantum walks with two absorbing boundaries, focusing on a specific initial condition [27]. Subsequent studies attempted to extend the analysis to more general initial conditions [28–31], although an exact treatment for arbitrary initial conditions remains to date elusive. Physically, absorbing boundaries represent measurement events [32–36], and in quantum mechanics, measurement is not a passive readout but dynamical intervention that nontrivially reshapes the system's evolution [37]. Quantum splitting probabilities therefore are not intrinsic to the system dynamics alone, but are also governed by these dynamical measurement interventions. Indeed, the sampling time, as defined later, serves as a tunable control parameter in state-of-the-art experiments based on quantum computers [38–40], optical waveguides [41–45] and trapped ions [46], which so far study the single-target detection problem [47–57].

How do quantum measurements shape outcomes among multiple competing targets? Which physical principles govern the competition? What nonclassical features emerge due to quantum fluctuations? The purpose of this Letter is to build an exact theory for the splitting probability of monitored *continuous-time* quantum walks. For a broad class of tight-binding Hamiltonians, we expose a quantum-superposition induced map-

* prashantsinghramitay@gmail.com

ping that connects the dual-target splitting problem to a pair of single-target detection problems. This mapping reveals (i) a nonanalytic structure of the splitting probability for special sampling times, (ii) a breakdown of the proximity effect, and (iii) the emergence of a phase-transition-like behavior at a critical sampling time, separating two qualitatively distinct splitting regimes. All these behaviors (i-iii) arise from the subtle interplay of quantum interference and measurement, standing in sharp contrast to both classical case in Eq. (1) and Hadamard quantum walks [27–31].

General formalism: We focus on a discrete-state, continuous-time quantum system characterized by a time-independent Hermitian Hamiltonian H , defined on a Hilbert space \mathcal{H} with a finite number of states N [58–62]. The dynamics is monitored at two distinct target states, $|x_L\rangle$ and $|x_R\rangle$, at regular time intervals τ , which define the sampling time of the dynamics. The target states satisfy the orthogonality condition $\langle x_L|x_R\rangle = 0$. The Hamiltonian could, for instance, represent the nearest-neighbor tight-binding model on a line

$$H = -\gamma \sum_{x=1}^{N-1} \left[|x\rangle\langle x+1| + |x+1\rangle\langle x| \right], \quad (2)$$

where γ is the hopping amplitude; see Fig. 1. We will return to this model later to illustrate the general results.

More generally, for an arbitrary Hamiltonian H describing a quantum walk on a graph with general target states $|x_L\rangle$ and $|x_R\rangle$, the time-evolution takes place in the following way:

1. Initialize the system in an arbitrary state $|\psi_0\rangle$.
2. Evolve it for a time duration τ via the unitary operator $U(\tau) = \exp(-iH\tau)$, where $\hbar = 1$.
3. At the end of this time, perform a projective measurement to check the system in the $|x_L\rangle$ target state. If detected, the process stops. Otherwise, the state is projected onto the subspace complementary to $|x_L\rangle$.
4. With this projected state, a second projective measurement is immediately performed to check the system in the second target state $|x_R\rangle$. If detected there, the process terminates. Otherwise, the state is projected onto the subspace complementary to $|x_R\rangle$.
5. Starting from this projected state, repeat steps (2–4).

We are interested in the splitting probability, *i.e.*, the probability that the system is eventually detected in one target before the other one. To this end, we repeat steps (2–4), in principle, for an infinite number of times or until a successful detection occurs at a target. Notice that after every measurement cycle, a projective measurement is first performed at $|x_L\rangle$ and subsequently at

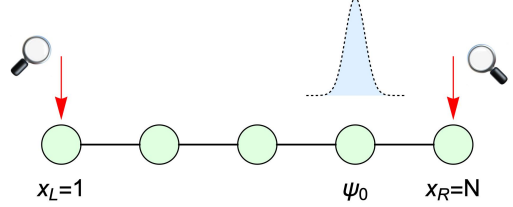


FIG. 1. A continuous-time quantum walk initially localized at $|\psi_0\rangle = |4\rangle$ moves on a tight-binding chain of size $N = 5$, with Hamiltonian in Eq. (2). Projective measurements are performed at $x_L = 1$ and $x_R = N$ at regular time intervals τ adopting the splitting protocol explained in the Letter. The goal is to determine the probabilities of detecting at the left and right.

$|x_R\rangle$. However, our results are insensitive to this ordering, and one may equally reverse the sequence without affecting any of the conclusions [63].

Splitting probability: Suppose that the measurement cycle is repeated n times (with $n \geq 1$). The probability that the system is first detected at time $t = n\tau$ at the $|x_\alpha\rangle$ target (with $\alpha \in \{L, R\}$), before any detection occurs at the other target state $|x_{\bar{\alpha}}\rangle$ (where $\bar{\alpha} = R$ if $\alpha = L$ and vice versa), is given by $F_n^{(\alpha)} = |\phi_n^{(\alpha)}|^2$, where [63]

$$\phi_n^{(\alpha)} = \langle x_\alpha | U(\tau) \mathcal{S}^{n-1} | \psi_0 \rangle. \quad (3)$$

Here, $\mathcal{S} = \left[\left(\mathbb{1} - |x_L\rangle\langle x_L| - |x_R\rangle\langle x_R| \right) U(\tau) \right]$ is the so-called survival operator [48–50], with $\mathbb{1}$ being the identity operator. It demonstrates unitary evolution in the time interval τ , followed by the complementary projection $\left(\mathbb{1} - |x_L\rangle\langle x_L| - |x_R\rangle\langle x_R| \right)$, indicating failed detections of both target states. In Eq. (3), the survival operator appears $(n-1)$ number of times describing the $(n-1)$ consecutive failed detections of the targets. During the final interval from $t = (n-1)\tau$ to $t = n\tau$, the system evolves unitarily, giving rise to the factor $U(\tau)$ in Eq. (3). We then perform the n th measurement sequentially, first probing $|x_L\rangle$ and, if no detection occurs, projecting with $(\mathbb{1} - |x_L\rangle\langle x_L|)$ before subsequently probing $|x_R\rangle$. Since $\langle x_R|x_L\rangle = 0$, this intermediate projection does not affect the amplitude, yielding Eq. (3) for both $|x_L\rangle$ and $|x_R\rangle$.

The quantity $\phi_n^{(\alpha)}$ thus can be interpreted as the first-detection amplitude of the $|x_\alpha\rangle$ state at the n -th measurement attempt before the other $|x_{\bar{\alpha}}\rangle$ state is detected. The corresponding splitting probability of detection is $P_\alpha(\psi_0) = \sum_{n=1}^{\infty} |\phi_n^{(\alpha)}|^2$. The sum accounts for the events of first detection occurring at the first, second, third measurements, and so on. For notational simplicity, we suppress the N and τ dependence in $P_\alpha(\psi_0)$.

Mapping to single-target problems: To enable a systematic comparison with the classical splitting probabilities in Eq. (1), we focus on the one-dimensional lattice system with N sites. We label the sites as $x \in \{1, 2, \dots, N\}$.

Arrival is monitored at the left and the right boundaries, $x_L = 1$ and $x_R = N$. We now show that $\phi_n^{(\alpha)}$ admits an exact mapping to a pair of single-target problems for a broad class of Hamiltonians.

To this end, we introduce two auxiliary orthogonal quantum states $|d_{\pm}\rangle = (|x_L\rangle \pm |x_R\rangle)/\sqrt{2}$. For $n = 1$, one can express Eq. (3) in terms of these states as $\phi_1^{(L)} = [\langle d_+|U(\tau)|\psi_0\rangle + \langle d_-|U(\tau)|\psi_0\rangle]/\sqrt{2}$, and similarly for the right boundary. Notice that $\phi_1^{(L)}$ decomposes into two separate terms $\langle d_{\pm}|U(\tau)|\psi_0\rangle$. Clearly, these terms are single-target amplitudes of detecting the system in states $|d_{\pm}\rangle$ in the first measurement [48–50].

For $n = 2$, the decomposition becomes more involved, $\phi_2^{(L)} = [(d_+|U(\tau)(\mathbb{1} - |d_+\rangle\langle d_+|)U(\tau)|\psi_0\rangle + \langle d_-|U(\tau)(\mathbb{1} - |d_-\rangle\langle d_-|)U(\tau)|\psi_0\rangle - \mathcal{M}]/\sqrt{2}$, where $\mathcal{M} = \langle d_+|U(\tau)|d_-\rangle\langle d_-|U(\tau)|\psi_0\rangle + \langle d_-|U(\tau)|d_+\rangle\langle d_+|U(\tau)|\psi_0\rangle$. Notice that \mathcal{M} involves matrix elements such as $\langle d_{\pm}|U(\tau)|d_{\mp}\rangle$. For a generic Hamiltonian, these elements are generally nonzero, and consequently \mathcal{M} does not vanish. However, for parity-symmetric Hamiltonians, we show in the Supplemental Material (SM) that $\langle d_{\pm}|U(\tau)|d_{\mp}\rangle = 0$ [64]. The parity operator is defined as $\mathcal{P}|x\rangle = |N+1-x\rangle$, corresponding to reflection about the center of the lattice system. For Hamiltonians satisfying this symmetry (*i.e.*, the commutation $[H, \mathcal{P}] = 0$), one gets $\mathcal{M} = 0$, and the above expression of $\phi_2^{(L)}$ reduces to a linear combination of two single-target detection amplitudes at $|d_{\pm}\rangle$ for $n = 2$.

In the SM [64], we use induction to show that such a decomposition is valid for generic n

$$\phi_n^{(L)} = (\chi_n^{(+)} + \chi_n^{(-)})/\sqrt{2}, \quad \phi_n^{(R)} = (\chi_n^{(+)} - \chi_n^{(-)})/\sqrt{2}, \quad (4)$$

where $\chi_n^{(\pm)} = \langle d_{\pm}|U(\tau)[(\mathbb{1} - |d_{\pm}\rangle\langle d_{\pm}|)U(\tau)]^{n-1}|\psi_0\rangle$.

The terms $\chi_n^{(\pm)}$ admit a direct interpretation in the single-target detection framework [48–50]. They represent the first-detection amplitudes for two auxiliary quantum systems, each stroboscopically monitored at a distinct single target state. For $\chi_n^{(+)}$, the auxiliary target state is $|d_+\rangle$, whereas for $\chi_n^{(-)}$, the dynamics is monitored at a different auxiliary target state $|d_-\rangle$. Eq. (4) is the mapping mentioned earlier. For parity-symmetric Hamiltonians, the detection amplitude $\phi_n^{(\alpha)}$ in Eq. (3) for the dual-target splitting problem is connected to the detection amplitudes of two distinct auxiliary single-target detection problems, each with its own target.

The mapping is a direct consequence of the quantum superposition principle, which permits the introduction of the quantum states $|d_{\pm}\rangle$. Such a construction has no classical analogue, since $|d_{\pm}\rangle$ cannot be interpreted as physical states in the classical probabilistic framework. Importantly, Eq. (4) provides a practical advantage: it enables us to use earlier methods from the single-target first detection setups [47–53] to obtain explicit formulas for the splitting probabilities, as we demonstrate later. From a physical perspective, the mapping implies an interference effect between the two single-target

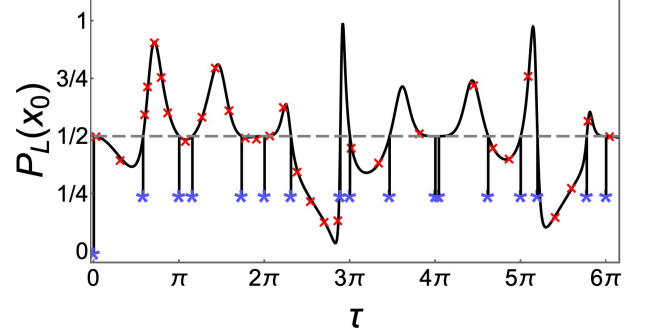


FIG. 2. Splitting probability at the left boundary as a function of τ for $x_0 = 4$ and $N = 5$. Red and blue symbols represent the numerical simulations with blue highlighting the resonant points. Black solid line corresponds to our analytical results in Eqs. (5) and (6). When $P_L(4) > 1/2$ (shown by the dashed line), the classical proximity effect is broken, as explained in the Letter.

detection processes, which can be either constructive or destructive. As we soon show, this interference leads to a phase-transition-like behavior in the splitting probabilities.

Tight-binding model with nearest-neighbor hops: For this case, the Hamiltonian takes the form in Eq. (2). Observe that H is parity symmetric, *i.e.*, $[H, \mathcal{P}] = 0$. Moreover, this Hamiltonian has been also implemented experimentally [38–45]. Throughout, we rescale time by $\gamma t/\hbar \rightarrow t$ (or equivalently, we set $\gamma = \hbar = 1$). Then, the dispersion relation becomes $E_k = -2 \cos(\omega_k)$ and the energy eigenfunction $\psi_k(x) = \langle x|E_k\rangle \propto \sin(\omega_k x)$, where $\omega_k = \pi k/(N+1)$, $k \in \{1, 2, \dots, N\}$ and $x \in \{1, 2, \dots, N\}$. For simplicity, we take the initial state $|\psi_0\rangle = |x_0\rangle$, where recall $x_0 \in \{1, 2, \dots, N\}$, $x_L = 1$ and $x_R = N$.

Dark States and the Splitting problem: Employing our mapping (4), we find that at certain values of τ , both $P_L(x_0)$ and $P_R(x_0)$ develop pointwise discontinuities (see the blue symbols in Fig. 2). At these points, the total detection probability drops below unity, $P_L(x_0) + P_R(x_0) < 1$. A finite fraction of realizations of the walk never triggers a detection at either boundary. Contrast this behavior with Eq. (1) where the sum is always equal to unity, since the underlying classical process is ergodic. We find that the discontinuities arise whenever the sampling time satisfies the condition

$$(E_k - E_{\ell})\tau = 0 \bmod 2\pi, \quad (5)$$

for any two distinct energies, E_k and E_{ℓ} , such that the corresponding energy eigenstates, $|E_k\rangle$ and $|E_{\ell}\rangle$, have the same parity under the reflection transformation introduced before. Resonances do not occur if their parities are different.

Physically, at special τ in Eq. (5), a dark state $|\mathcal{D}\rangle$ is created in the system, that is orthogonal to both boundaries, $\langle x_L|\mathcal{D}\rangle = \langle x_R|\mathcal{D}\rangle = 0$, at the measurement instances. The process of repeated measurements can drive

the system to this state, thus creating a non-detectable state and hence the splitting probabilities sum is less than unity. More specifically, if the initial state has a finite overlap with this state, $\langle \mathcal{D} | x_0 \rangle \neq 0$, then Eq. (5) implies that the system evolves in such a way that a component of its wave function becomes dark at the measurement times $t = \tau, 2\tau, 3\tau, \dots$ [63]. That is, this component is decoupled from both boundaries at the moments of measurement. As a consequence, the splitting probabilities exhibit sharp suppressions. Moreover, since this portion of the wave function is never detected at the boundaries, the total detection probability is less than one, as mentioned before. In Fig. 2, we verify the resonances using numerical simulations for $x_0 = 4$ and $N = 5$ (see the End Matter for details).

Loss of proximity effect: For generic (non-resonant) values of τ , the splitting probabilities depend smoothly on τ (see the red symbols in Fig. 2), and satisfy the normalization condition $P_L(x_0) + P_R(x_0) = 1$. Their expressions are

$$P_L(x_0) = \frac{1}{2} + \xi(x_0, N, \tau), \quad P_R(x_0) = \frac{1}{2} - \xi(x_0, N, \tau), \quad (6)$$

where the function $\xi(x_0, N, \tau)$ represents the interference effect between the single-target detection amplitudes χ_n^\pm in Eq. (4). It can be computed exactly and is provided in Eq. (EM6) at the End Matter. For example, when $x_0 = 4$ and $N = 5$, we get

$$\xi(4, 5, \tau) = -\frac{\sqrt{3} \sin\left(\frac{\tau}{2}\right)^2 \sin(\tau) \sin(\sqrt{3}\tau)}{4 + \cos(2\tau) + \cos(\tau) \left[-1 + \cos(\sqrt{3}\tau) \{ -5 + \cos(\tau) \} \right]}. \quad (7)$$

As shown in Fig. 2, over a wide range of τ values, we find $P_L(4) > 1/2$, and hence $P_R(x_0) < 1/2$ according to Eq. (6); see the dashed line in the figure. Thus, the proximity effect is lost, $P_R(4) < P_L(4)$, even though the walker ($x_0 = 4$) is initially closer to the right boundary ($x_R = 5$). This behavior contrasts with the classical case in Eq. (1).

Flat-to-fluctuating transition for large system size: We now turn to the sampling transition that was mentioned before. Fig. 3 shows the plot of $P_L(x_0)$ as a function of τ using Eq. (6) for two initial conditions, $x_0 = 11$ and $x_0 = 30$, keeping the system size fixed at $N = 400$ for both. For $N \gg 1$, the splitting probability undergoes a surprising change in behavior at a critical sampling time $\tau_c = \pi/2$, shown by the dashed vertical line in Fig. 3. This critical value, as shown later, is related to the width of the energy band. In the regime $0 < \tau \leq \tau_c$, the splitting probability is essentially equal to $1/2$, independent of the sampling time. Moreover, this flat result is the same for both values of x_0 in Fig. 3, indicating that it is also independent of the initial condition. Thus, the splitting probability displays a robust and universal flat behavior with a value essentially equal to $1/2$ in this regime.

Beyond this critical point, $\tau > \tau_c$, a qualitatively different, non-universal behavior emerges. Here, $P_L(x_0)$ deviates from $1/2$, and develops a fluctuating pattern with

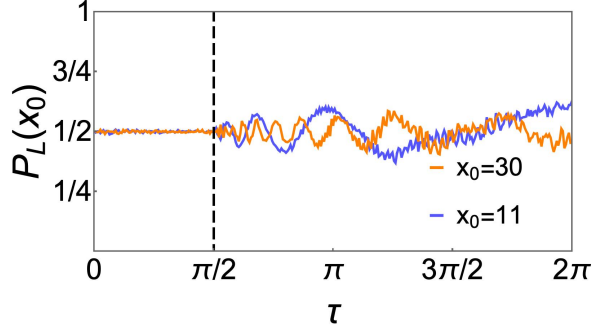


FIG. 3. Flat-to-fluctuating transition of the splitting probability at $\tau_c = \pi/2$ for two initial conditions, $x_0 = 11$ and $x_0 = 30$ with $N = 400$ using Eq. (6). Resonances at special values of τ , given in Eq. (5), are omitted for clarity.

pronounced peaks and dips as the sampling time is varied. These features are not universal and depend on both x_0 and τ . Thus, as τ crosses τ_c , $P_L(x_0)$ changes its behavior from a universal flat behavior to a fluctuating, non-universal behavior. The same transition is observed for $P_R(x_0)$ [63]. In contrast, a classical random walk does not exhibit such a transition. To gain some insight into this behavior, we start with an analysis of the Zeno limit.

Small- τ analysis: From a mathematical standpoint, when τ is small but finite ($0 < \tau \ll 1$), we can perform a perturbative analysis in τ to obtain $\xi(x_0, N, \tau) \simeq (\delta_{x_0, 1} - \delta_{x_0, N})/2$ for general N [63]. Plugging this result in Eq. (6) yields $P_L(x_0) \simeq P_R(x_0) \simeq 1/2$ for any initial condition in the bulk ($1 < x_0 < N$). On the boundaries, we have $P_L(x_0 = 1) \simeq 1$ and $P_L(x_0 = N) \simeq 0$ (and similarly for $P_R(x_0)$) as $\tau \rightarrow 0$, since for $x_0 = 1$, the particle is always detected at the left boundary, whereas for $x_0 = N$, it is always detected at the right boundary (and never at the left boundary). For all other x_0 , the splitting probabilities take on a flat value of $1/2$. This perturbative result is consistent with the flat behavior observed in the $0 < \tau \leq \tau_c$ regime in Fig. 3.

Our Zeno result is in stark contrast with the classical case in Eq. (1), where splitting probabilities depend linearly on x_0 . Physically, the flatness stems from the fact that, for small τ , the quantum walker is mostly confined in the bulk, with only a small probability ($\sim \tau^2$) of being detected at the boundaries during each measurement attempt. As a result, it typically requires many attempts before being detected, and over this long sequence of measurements, any memory of the initial positional asymmetry is effectively erased. This explains the flatness of the splitting probability at small τ , yet does not explain the transition at τ_c .

Spectral origin of the transition: Eq. (6) shows that deviations of the splitting probabilities from $1/2$ originate from the term $\xi(x_0, N, \tau)$. The key point is that $\xi(x_0, N, \tau)$ is controlled by the eigenvalues $\{\lambda_-\}$ of the survival operator $\mathcal{S}_- = (\mathbb{1} - |d_-\rangle \langle d_-|) U(\tau)$ in Eq. (4) (see SM [64] for details). Each λ_- yields an individual contribution, and $\xi(x_0, N, \tau)$ is determined by their

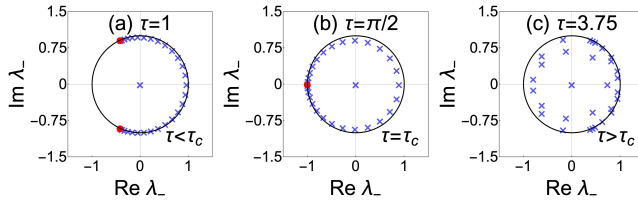


FIG. 4. Eigenvalues $\{\lambda_-\}$ (in blue) of the survival operator $S_- = (\mathbb{1} - |d_- \rangle \langle d_-|) U(\tau)$ in Eq. (4) for (a) $\tau = 1$ ($\tau < \tau_c$), (b) $\tau = \pi/2$ ($\tau = \tau_c$) and (c) $\tau = 3.75$ ($\tau > \tau_c$) with $N = 61$. In (a-b), the two red points represent $a_1(\tau) = \exp(-iE_{\min}\tau)$ and $a_2(\tau) = \exp(-iE_{\max}\tau)$, as explained in the Letter. For $x_0 = 11$, we find $\xi(x_0, N, \tau = 1) \approx 0.002$, $\xi(x_0, N, \tau = \tau_c) \approx -0.002$ and $\xi(x_0, N, \tau = 3.75) \approx -0.135$.

combined sum. In contrast, the eigenvalues of $S_+ = (\mathbb{1} - |d_+ \rangle \langle d_+|) U(\tau)$ do not control $\xi(x_0, N, \tau)$ [64].

For $\tau \leq \tau_c$ and large system sizes, we find in Fig. 4(a) (in blue) that all $\{\lambda_-\}$, except the one at the origin, are arranged regularly along a single arc close to $|z| = 1$, between the points $a_1(\tau)$ and $a_2(\tau)$ (in red). By inspection, we find $a_1(\tau) = \exp(-iE_{\min}\tau)$ and $a_2(\tau) = \exp(-iE_{\max}\tau)$, where $E_{\min} \approx -2$ and $E_{\max} \approx 2$ are the minimum and maximum eigenvalues of H in Eq. (2). Because of the regular arrangement of $\{\lambda_-\}$ in the complex plane, their individual contributions to $\xi(x_0, N, \tau)$ largely cancel with each other, yielding a negligible sum, *i.e.* $\xi(x_0, N \gg 1, \tau \leq \tau_c) \approx 0$. Eq. (6) then implies $P_L(x_0) \approx P_R(x_0) \approx 1/2$.

This behavior persists till the critical sampling time

$$\Delta E \tau_c = 2\pi, \quad (8)$$

with $\Delta E = (E_{\max} - E_{\min}) = 4$ (*i.e.*, $\tau_c = \pi/2$ as pointed out before), the two endpoints meet, $a_1(\tau) = a_2(\tau) = -1$, and the arc closes (Fig. 4(b)).

Increasing τ further, the endpoints move past each other, and $\{\lambda_-\}$ are no longer confined to a single arc; see Fig. 4(c). Instead, their arrangement becomes irregular in the complex plane, with eigenvalues spreading nonuniformly inside the unit disk. As a result, the contributions associated with different λ_- no longer cancel,

and $\xi(x_0, N \gg 1, \tau > \tau_c) \neq 0$. This leads to the departure of the splitting probabilities from their flat value of 1/2 via Eq. (6) for $\tau > \tau_c$. In this way, the transition in the splitting probabilities is directly linked to the qualitative reorganization of the eigenvalues $\{\lambda_-\}$ as τ crosses τ_c (see SM [64] for further details).

Experimental outlook: Our results can be tested experimentally. In quantum computers [38–40], for instance, quantum walks can be implemented using qubits, and mid-circuit measurements enable periodic detection on a selected subset of qubits corresponding to the target sites during the evolution. Similarly, in photonic waveguides [41–45], quantum walks can be effectively implemented by using electric fields across an array of coupled waveguides, and periodic measurements can be realized using a series of segmented waveguides. Very recently, quantum first-passage-time distributions were also measured using a harmonically trapped ion, where periodic measurement was implemented via controlled laser pulses [46]. These setups provide direct experimental platforms to probe the splitting dynamics and the flat-to-fluctuating transition predicted here. Notably, observing this transition does not require very large system sizes, and the effect already appears for moderate values of N [63], making it amenable for experiments.

Conclusion: We have shown that the splitting probability of a continuous-time quantum walk exhibits a sharp transition from a universal regime where it is equal to 1/2, independent of the initial position and the sampling time to a non-universal regime, where it has fluctuating structures. This result is in stark contrast to the splitting probabilities of classical random walks [2–4] and of discrete-time Hadamard walks [27–31]. The transition is a manifestation of the qualitative change in the arrangement of eigenvalues of the associated survival operators. Notably, the critical point τ_c is dependent only on the width of the energy band. Therefore, the transition is likely to go beyond the studied model and to hold generically for a wide class of Hamiltonians. Other nonclassical features include the breakdown of the proximity effect and the emergence of special sampling times that drive the system to dark states, rendering discontinuous jumps in the splitting probability.

Acknowledgment: This research was supported by the Israel Science Foundation (grant No. 2311/25).

End Matter

General Expressions of $P_L(x_0)$ and $P_R(x_0)$

In Eq. (4), we explained that the detection amplitudes, $\phi_n^{(L)}$ and $\phi_n^{(R)}$, are mapped to two auxiliary single-target detection amplitudes $\chi_n^{(\pm)} = \langle d_{\pm} | U(\tau) [(1 - |d_{\pm} \rangle \langle d_{\pm}|) U(\tau)]^{n-1} | x_0 \rangle$. Summing the squared moduli of the first-detection

amplitudes over n yields the splitting probabilities

$$P_L(x_0) = \sum_{n=1}^{\infty} |\phi_n^{(L)}|^2 = \frac{1}{2} [\rho_+(x_0) + \rho_-(x_0)] + \operatorname{Re} \left[\sum_{n=1}^{\infty} \chi_n^{(+)} \left(\chi_n^{(-)} \right)^* \right], \quad (\text{EM1})$$

$$P_R(x_0) = \sum_{n=1}^{\infty} |\phi_n^{(R)}|^2 = \frac{1}{2} [\rho_+(x_0) + \rho_-(x_0)] - \operatorname{Re} \left[\sum_{n=1}^{\infty} \chi_n^{(+)} \left(\chi_n^{(-)} \right)^* \right]. \quad (\text{EM2})$$

Here, $\rho_{\pm}(x_0) = \sum_{n=1}^{\infty} |\chi_n^{(\pm)}|^2$ are the total detection probabilities in the auxiliary problems. Single-target detection problems of this type have been extensively studied before [47–53]. Leveraging these methods within our mapping, we get $\rho_{\pm}(x_0)$ that appear in Eqs. (EM1) and (EM2). For the Hamiltonian in Eq. (2) and non-special τ (i.e., τ not satisfying Eq. (5)), we find [63]

$$\rho_+(x_0) = \sum_{\substack{k=1 \\ k \in \text{odd}}}^N |\langle E_k | x_0 \rangle|^2, \quad \rho_-(x_0) = \sum_{\substack{k=1 \\ k \in \text{even}}}^N |\langle E_k | x_0 \rangle|^2. \quad (\text{EM3})$$

where $|E_k\rangle$ is the energy eigenstate. To obtain the interference part in Eqs. (EM1) and (EM2), it is instructive to introduce the auxiliary generating functions $\tilde{\chi}^{(\pm)}(z) = \sum_{n=1}^{\infty} z^n \chi_n^{(\pm)}$. Using earlier methods [50, 53], we can write them as [63]

$$\tilde{\chi}^{(+)}(z) = \frac{\sum_{k \in \text{odd}} \sin(\omega_k) \sin(\omega_k x_0) \left(\frac{e^{2i\tau \cos(\omega_k)}}{1-z e^{2i\tau \cos(\omega_k)}} \right)}{\sum_{k \in \text{odd}} \sin^2(\omega_k) \left(\frac{1}{1-z e^{2i\tau \cos(\omega_k)}} \right)}, \quad \tilde{\chi}^{(-)}(z) = \frac{\sum_{k \in \text{even}} \sin(\omega_k) \sin(\omega_k x_0) \left(\frac{e^{2i\tau \cos(\omega_k)}}{1-z e^{2i\tau \cos(\omega_k)}} \right)}{\sum_{k \in \text{even}} \sin^2(\omega_k) \left(\frac{1}{1-z e^{2i\tau \cos(\omega_k)}} \right)}, \quad (\text{EM4})$$

where $\omega_k = \pi k / (N+1)$. In terms of these generating functions, the interference term in Eqs. (EM1) and (EM2) can be expressed as

$$\xi(x_0, N, \tau) = \operatorname{Re} \left[\sum_{n=1}^{\infty} \chi_n^{(+)} \left(\chi_n^{(-)} \right)^* \right] = \operatorname{Re} \left[\oint_{|z|=1} \frac{dz}{2\pi iz} \tilde{\chi}^{(+)}(z) \left(\tilde{\chi}^{(-)}(1/z) \right)^* \right]. \quad (\text{EM5})$$

This relation makes it explicit that $\xi(x_0, N, \tau)$ represents the interference effect between the two single-target detection processes. Plugging Eq. (EM4)

$$\xi(x_0, N, \tau) = \operatorname{Re} \left[\oint_{|z|=1} dz \mathcal{I}(z, x_0, N, \tau) \right], \quad \text{with} \quad (\text{EM6})$$

$$\mathcal{I}(z, x_0, N, \tau) = \frac{1}{2\pi iz} \left[\frac{\sum_{k \in \text{odd}} \sin(\omega_k) \sin(\omega_k x_0) \left(\frac{e^{2i\tau \cos(\omega_k)}}{1-z e^{2i\tau \cos(\omega_k)}} \right)}{\sum_{k \in \text{odd}} \sin^2(\omega_k) \left(\frac{1}{1-z e^{2i\tau \cos(\omega_k)}} \right)} \right] \left[\frac{\sum_{k \in \text{even}} \sin(\omega_k) \sin(\omega_k x_0) \left(\frac{e^{-2i\tau \cos(\omega_k)}}{z e^{-2i\tau \cos(\omega_k)}} \right)}{\sum_{k \in \text{even}} \sin^2(\omega_k) \left(\frac{1}{z e^{-2i\tau \cos(\omega_k)}} \right)} \right]. \quad (\text{EM7})$$

Combining Eqs. (EM3) and (EM6), we obtain

$$P_L(x_0) = \frac{1}{2} + \xi(x_0, N, \tau), \quad P_R(x_0) = \frac{1}{2} - \xi(x_0, N, \tau), \quad (\text{EM8})$$

which was quoted in the Letter. Eqs. (EM6–EM8) give the splitting probabilities for all values of x_0 , τ and N (except at the special sampling times). For $x_0 = 4$, $N = 5$, Eqs. (EM6–EM7) take a simple form

$$\xi(4, 5, \tau) = -\frac{\sqrt{3} \sin\left(\frac{\tau}{2}\right)^2 \sin(\tau) \sin(\sqrt{3}\tau)}{4 + \cos(2\tau) + \cos(\tau) \left[-1 + \cos(\sqrt{3}\tau) \{ -5 + \cos(\tau) \} \right]}. \quad (\text{EM9})$$

Finally, we turn to the special τ values given by Eq. (5). At these special points, a separate analysis is required, involving the eigenfunctions of the unitary operator $U(t) = \exp(-iHt)$, and their associated quasi-energies [63]. For $x_0 = 4$, $N = 4$, resonances occur at (i) $\tau = 0$, where $P_L(4) = P_R(4) = 0$; (ii) $\tau = m\pi$ ($m = 1, 2, 3, \dots$), where

$P_L(4) = P_R(4) = 1/4$; and (iii) $\tau = m\pi\sqrt{3}$, again with $P_L(4) = P_R(4) = 1/4$. All of them have $P_L(4) + P_R(4) < 1$. As explained before, this occurs because a part of the system enters into the darkspace that is decoupled from the two detectors at the measurement instances, thereby reducing the overall detection probability. These results have been shown in blue in Fig. 2 in the Letter.

[1] E. Shoesmith, Huygens' solution to the gambler's ruin problem, *Historia Mathematica* **13**, 157 (1986).

[2] W. Feller, *An Introduction to Probability Theory and its Applications* (Wiley, 1968).

[3] S. Redner, *A Guide to First-Passage Processes* (Cambridge University Press, 2001).

[4] S. N. Majumdar, A. Rosso, and A. Zoia, Hitting probability for anomalous diffusion processes, *Phys. Rev. Lett.* **104**, 020602 (2010).

[5] S. Condamin, V. Tejedor, R. Voituriez, O. Bénichou, and J. Klafter, Probing microscopic origins of confined sub-diffusion by first-passage observables, *Proceedings of the National Academy of Sciences* **105**, 5675 (2008).

[6] J. D. Chodera and V. S. Pande, Splitting probabilities as a test of reaction coordinate choice in single-molecule experiments, *Phys. Rev. Lett.* **107**, 098102 (2011).

[7] A. P. Manuel, J. Lambert, and M. T. Woodside, Reconstructing folding energy landscapes from splitting probability analysis of single-molecule trajectories, *Proceedings of the National Academy of Sciences* **112**, 7183 (2015).

[8] E. Roldán, I. Neri, M. Dörpinghaus, H. Meyr, and F. Jülicher, Decision making in the arrow of time, *Phys. Rev. Lett.* **115**, 250602 (2015).

[9] G. Oshanin and S. Redner, Helix or coil? fate of a melting heteropolymer, *Europhysics Letters* **85**, 10008 (2009).

[10] J. Klinger, R. Voituriez, and O. Bénichou, Splitting probabilities of symmetric jump processes, *Phys. Rev. Lett.* **129**, 140603 (2022).

[11] A. Vezzani and R. Burioni, Fast rare events in exit times distributions of jump processes, *Phys. Rev. Lett.* **132**, 187101 (2024).

[12] L. Claudio-Pachecano, H. Larralde, and C. Mejía-Monasterio, From anomalous diffusion in polygons to a transport locking relation, *Phys. Rev. E* **112**, 014107 (2025).

[13] S. Kalaj, E. Marinari, G. Oshanin, and L. Peliti, One-dimensional lattice random walks in a gaussian random potential, [arXiv:2509.23985](https://arxiv.org/abs/2509.23985) (2025).

[14] S. Belan, Restart could optimize the probability of success in a bernoulli trial, *Phys. Rev. Lett.* **120**, 080601 (2018).

[15] A. Chechkin and I. M. Sokolov, Random search with resetting: A unified renewal approach, *Phys. Rev. Lett.* **121**, 050601 (2018).

[16] M. Radice, Effects of mortality on stochastic search processes with resetting, *Phys. Rev. E* **107**, 024136 (2023).

[17] S. Bose, Quantum communication through an unmodulated spin chain, *Phys. Rev. Lett.* **91**, 207901 (2003).

[18] S. Bose, Quantum communication through spin chain dynamics: an introductory overview, *Contemporary Physics* **48**, 13 (2007).

[19] A. Bottarelli, M. Frigerio, and M. G. A. Paris, Quantum routing of information using chiral quantum walks, *AVS Quantum Science* **5**, 025001 (2023).

[20] H. Kristjánsson, Y. Zhong, A. Munson, and G. Chiribella, Quantum networks with coherent routing of information through multiple nodes, *npj Quantum Information* **10**, 131 (2024).

[21] A. M. Childs, Universal computation by quantum walk, *Phys. Rev. Lett.* **102**, 180501 (2009).

[22] F. Magniez, A. Nayak, J. Roland, and M. Santha, Search via quantum walk, *SIAM Journal on Computing* **40**, 142 (2011).

[23] G. A. Bezerra, P. H. G. Lugão, and R. Portugal, Quantum-walk-based search algorithms with multiple marked vertices, *Phys. Rev. A* **103**, 062202 (2021).

[24] J. Guan, Q. Wang, and M. Ying, An HHL-based algorithm for computing hitting probabilities of quantum walks, *Quantum Information & Computation* **21**, 395 (2021).

[25] H. Sahu and K. Sen, Quantum-walk search in motion, *Scientific Reports* **14**, 2815 (2024).

[26] C.-Y. Lu, W.-B. Gao, J. Zhang, X.-Q. Zhou, T. Yang, and J.-W. Pan, Experimental quantum coding against qubit loss error, *Proceedings of the National Academy of Sciences* **105**, 11050 (2008).

[27] A. Ambainis, E. Bach, A. Nayak, A. Vishwanath, and J. Watrous, One-dimensional quantum walks, in *Proceedings of the Thirty-Third Annual ACM Symposium on Theory of Computing*, STOC '01 (Association for Computing Machinery, New York, NY, USA, 2001) p. 37–49.

[28] E. Bach, S. Coppersmith, M. P. Goldschen, R. Joynt, and J. Watrous, One-dimensional quantum walks with absorbing boundaries, *Journal of Computer and System Sciences* **69**, 562 (2004).

[29] E. Bach and L. Borisov, Absorption probabilities for the two-barrier quantum walk, [arXiv:0901.4349](https://arxiv.org/abs/0901.4349) (2009).

[30] P. Kukliński and M. Kon, Absorption probabilities of quantum walks, *Quantum Information Processing* **17**, 263 (2018).

[31] Z. Ammara, V. Potoček, M. Štefaňák, and F. V. Pepe, Quantum walk on a line with absorbing boundaries, [arXiv:2508.13318](https://arxiv.org/abs/2508.13318) (2025).

[32] J. Kempe, Quantum random walks: An introductory overview, *Contemporary Physics* **44**, 307 (2003).

[33] N. Shenvi, J. Kempe, and K. B. Whaley, Quantum random-walk search algorithm, *Phys. Rev. A* **67**, 052307 (2003).

[34] H. Krovi and T. A. Brun, Hitting time for quantum walks on the hypercube, *Phys. Rev. A* **73**, 032341 (2006).

[35] S. Goswami, P. Sen, and A. Das, Quantum persistence: A random-walk scenario, *Phys. Rev. E* **81**, 021121 (2010).

[36] P. L. Krapivsky, J. M. Luck, and K. Mallick, Survival of classical and quantum particles in the presence of traps, *Journal of Statistical Physics* **154**, 1430 (2014).

[37] C. Cohen-Tannoudji, B. Diu, and F. Laloë, *Quantum Mechanics* (Wiley, 1973).

chanics (John Wiley & Sons, New York, NY, 1977).

[38] S. Tornow and K. Ziegler, Measurement-induced quantum walks on an IBM quantum computer, *Phys. Rev. Res.* **5**, 033089 (2023).

[39] Q. Wang, S. Ren, R. Yin, K. Ziegler, E. Barkai, and S. Tornow, First hitting times on a quantum computer: Tracking vs. local monitoring, topological effects, and dark states, *Entropy* **26**, 869 (2024).

[40] R. Yin, Q. Wang, S. Tornow, and E. Barkai, Restart uncertainty relation for monitored quantum dynamics, *Proceedings of the National Academy of Sciences* **122**, e2402912121 (2025).

[41] H. B. Perets, Y. Lahini, F. Pozzi, M. Sorel, R. Morandotti, and Y. Silberberg, Realization of quantum walks with negligible decoherence in waveguide lattices, *Phys. Rev. Lett.* **100**, 170506 (2008).

[42] M. Segev, Y. Silberberg, and D. N. Christodoulides, Anderson localization of light, *Nature Photonics* **7**, 197 (2013).

[43] H. Tang, X.-F. Lin, Z. Feng, J.-Y. Chen, J. Gao, K. Sun, C.-Y. Wang, P.-C. Lai, X.-Y. Xu, Y. Wang, L.-F. Qiao, A.-L. Yang, and X.-M. Jin, Experimental two-dimensional quantum walk on a photonic chip, *Science Advances* **4**, eaat3174 (2018).

[44] Q. Liu, W. Liu, K. Ziegler, and F. Chen, Engineering of zeno dynamics in integrated photonics, *Phys. Rev. Lett.* **130**, 103801 (2023).

[45] Q. Liu, W. Liu, Y. Jia, K. Ziegler, A. Alù, and F. Chen, Measurement-induced photonic topological insulators, *Science Advances* **11**, eadx0595 (2025).

[46] J. M. Ryan, S. Gorbaty, T. J. Kessler, M. G. Peaks, S. W. Teitsworth, and C. Noel, Experimental measurement of quantum-first-passage-time distributions, *arXiv:2508.21790* (2025).

[47] F. A. Grünbaum, L. Velázquez, A. H. Werner, and R. F. Werner, Recurrence for discrete time unitary evolutions, *Communications in Mathematical Physics* **320**, 543 (2013).

[48] S. Dhar, S. Dasgupta, and A. Dhar, Quantum time of arrival distribution in a simple lattice model, *Journal of Physics A: Mathematical and Theoretical* **48**, 115304 (2015).

[49] S. Dhar, S. Dasgupta, A. Dhar, and D. Sen, Detection of a quantum particle on a lattice under repeated projective measurements, *Phys. Rev. A* **91**, 062115 (2015).

[50] H. Friedman, D. A. Kessler, and E. Barkai, Quantum walks: The first detected passage time problem, *Phys. Rev. E* **95**, 032141 (2017).

[51] F. Thiel, E. Barkai, and D. A. Kessler, First detected arrival of a quantum walker on an infinite line, *Phys. Rev. Lett.* **120**, 040502 (2018).

[52] R. Yin, K. Ziegler, F. Thiel, and E. Barkai, Large fluctuations of the first detected quantum return time, *Phys. Rev. Res.* **1**, 033086 (2019).

[53] F. Thiel, I. Mualem, D. Meidan, E. Barkai, and D. A. Kessler, Dark states of quantum search cause imperfect detection, *Phys. Rev. Res.* **2**, 043107 (2020).

[54] D. Das and S. Gupta, Quantum random walk and tight-binding model subject to projective measurements at random times, *Journal of Statistical Mechanics: Theory and Experiment* **2022**, 033212 (2022).

[55] M. Kulkarni and S. N. Majumdar, First detection probability in quantum resetting via random projective measurements, *Journal of Physics A: Mathematical and Theoretical* **56**, 385003 (2023).

[56] B. Walter, G. Perfetto, and A. Gambassi, Thermodynamic phases in first detected return times of quantum many-body systems, *Phys. Rev. A* **111**, L040202 (2025).

[57] D. Soldner, I. Lesanovsky, and G. Perfetto, Nonanalyticities and ergodicity breaking in noninteracting many-body dynamics via stochastic resetting and global measurements, *arXiv:2510.11450* (2025).

[58] E. Farhi and S. Gutmann, Quantum computation and decision trees, *Phys. Rev. A* **58**, 915 (1998).

[59] A. M. Childs and J. Goldstone, Spatial search by quantum walk, *Phys. Rev. A* **70**, 022314 (2004).

[60] O. Mülken and A. Blumen, Continuous-time quantum walks: Models for coherent transport on complex networks, *Physics Reports* **502**, 37 (2011).

[61] S. E. Venegas-Andraca, Quantum walks: a comprehensive review, *Quantum Information Processing* **11**, 1015 (2012).

[62] J. Tabanera-Bravo and A. Godec, Purely quantum memory in closed systems observed via imperfect measurements, *Quantum* **9**, 1938 (2025).

[63] P. Singh, D. A. Kessler, and E. Barkai, To be published.

[64] P. Singh, D. A. Kessler, and E. Barkai, Supplementary material (2026).

SUPPLEMENTARY MATERIAL: TRANSITION IN SPLITTING PROBABILITIES OF QUANTUM WALKS

Prashant Singh, David A. Kessler and Eli Barkai
Department of Physics, Bar-Ilan University, Ramat Gan 52900, Israel

The Supplementary Material contains the derivation of the mapping to single-target detection in Sec. I, analysis of the eigenvalues of the survival operators in Sec. II, relation of the splitting probability with these eigenvalues in Sec. III, and discussion on the spectral origin of the transition in the splitting probability in Sec. IV.

I. DERIVATION OF THE MAPPING TO SINGLE-TARGET DETECTION

In the Letter, we pointed out that the first-detection amplitude $\phi_n^{(\alpha)}$ for detection at boundary x_α ($\alpha \in \{L, R\}$), given the absence of detection at the opposite boundary $x_{\bar{\alpha}}$ (with $\bar{\alpha} = R$ for $\alpha = L$ and vice versa), satisfies a quantum mapping for the parity-symmetric Hamiltonians. This mapping connects the dual-target detection amplitudes to two distinct auxiliary single-target first-detection amplitudes $\chi_n^{(\pm)}$ as follows

$$\phi_n^{(L)} = \frac{(\chi_n^{(+)} + \chi_n^{(-)})}{\sqrt{2}}, \quad \phi_n^{(R)} = \frac{(\chi_n^{(+)} - \chi_n^{(-)})}{\sqrt{2}}, \quad (\text{SM1})$$

where amplitudes $\chi_n^{(\pm)}$ are given by

$$\chi_n^{(\pm)} = \langle d_\pm | U(\tau) \left[(\mathbb{1} - |d_\pm\rangle\langle d_\pm|) U(\tau) \right]^{n-1} |\psi_0\rangle. \quad (\text{SM2})$$

Here $U(\tau) = \exp(-iH\tau)$, $|d_\pm\rangle = (|x_L\rangle \pm |x_R\rangle)/\sqrt{2}$, $|x_L\rangle = 1$ and $|x_R\rangle = N$. Before deriving Eq. (SM1), we recall some basic properties of the parity (reflection) operator \mathcal{P} , defined by its action on the position basis as

$$\mathcal{P} |x\rangle = |N+1-x\rangle. \quad (\text{SM3})$$

The parity operator is its own inverse, $\mathcal{P}^{-1} = \mathcal{P}$, and satisfies $\mathcal{P}^2 = \mathbb{1}$. For Hamiltonians possessing the reflection symmetry, the parity operator commutes with the Hamiltonian

$$[H, \mathcal{P}] = 0, \quad \implies \quad \mathcal{P} H \mathcal{P} = H. \quad (\text{SM4})$$

As a consequence, the unitary operator also satisfies

$$\mathcal{P} U(\tau) \mathcal{P} = U(\tau). \quad (\text{SM5})$$

We also have $\mathcal{P} |d_\pm\rangle = \pm |d_\pm\rangle$. Combining this relation with Eq. (SM5) gives

$$\langle d_+ | U(\tau) | d_- \rangle = \langle d_- | U(\tau) | d_+ \rangle = 0, \quad (\text{SM6})$$

for the parity-symmetric Hamiltonians. With these results at disposal, we proceed to derive the mapping in Eq. (SM1).

Let us analyze the expression of $\phi_n^{(\alpha)}$ given in the Letter

$$\phi_n^{(\alpha)} = \langle x_\alpha | U(\tau) \left[(\mathbb{1} - |x_L\rangle\langle x_L| - |x_R\rangle\langle x_R|) U(\tau) \right]^{n-1} |\psi_0\rangle, \quad \alpha \in \{L, R\}. \quad (\text{SM7})$$

For $n = 1$, $\phi_n^{(L)}$ and $\phi_n^{(R)}$ readily satisfy Eq. (SM1). On the other hand, for $n = 2$, one gets

$$\phi_2^{(L)} = \frac{1}{\sqrt{2}} \left[\chi_2^{(+)} + \chi_2^{(-)} - \langle d_+ | U(\tau) | d_- \rangle \langle d_- | U(\tau) | \psi_0 \rangle - \langle d_- | U(\tau) | d_+ \rangle \langle d_+ | U(\tau) | \psi_0 \rangle \right], \quad (\text{SM8})$$

$$\phi_2^{(R)} = \frac{1}{\sqrt{2}} \left[\chi_2^{(+)} - \chi_2^{(-)} - \langle d_+ | U(\tau) | d_- \rangle \langle d_- | U(\tau) | \psi_0 \rangle + \langle d_- | U(\tau) | d_+ \rangle \langle d_+ | U(\tau) | \psi_0 \rangle \right]. \quad (\text{SM9})$$

Substituting Eq. (SM6), we see that Eqs. (SM8) and (SM9) reduce to our mapping in Eq. (SM1). Hence, the mapping is satisfied for $n = 2$.

We now use induction to prove that Eq. (SM1) holds for general n . Assume that the mapping is valid for $n = m$. Then

$$\begin{aligned} \langle x_L | U(\tau) \left[\left(\mathbb{1} - |x_L\rangle \langle x_L| - |x_R\rangle \langle x_R| \right) U(\tau) \right]^{m-1} &= \frac{1}{\sqrt{2}} \left[\langle d_+ | U(\tau) \left[\left(\mathbb{1} - |d_+\rangle \langle d_+| \right) U(\tau) \right]^{m-1} \right. \\ &\quad \left. + \langle d_- | U(\tau) \left[\left(\mathbb{1} - |d_-\rangle \langle d_-| \right) U(\tau) \right]^{m-1} \right], \end{aligned} \quad (\text{SM10})$$

where we have focused on the left boundary for simplicity. The derivation for the right one proceeds analogously. We plug this relation in Eq. (SM7) for $n = (m + 1)$ to yield

$$\begin{aligned} \phi_{m+1}^{(L)} &= \frac{1}{\sqrt{2}} \left[\chi_{m+1}^{(+)} + \chi_{m+1}^{(-)} - \langle d_+ | U(\tau) \left[\left(1 - |d_+\rangle \langle d_+| \right) U(\tau) \right]^{m-1} |d_-\rangle \langle d_- | U(\tau) | \psi_0 \rangle \right. \\ &\quad \left. - \langle d_- | U(\tau) \left[\left(1 - |d_-\rangle \langle d_-| \right) U(\tau) \right]^{m-1} |d_+\rangle \langle d_+ | U(\tau) | \psi_0 \rangle \right]. \end{aligned} \quad (\text{SM11})$$

Since the projector $|d_{\pm}\rangle \langle d_{\pm}|$ is parity invariant, the operator $U(\tau)[(\mathbb{1} - |d_{\pm}\rangle \langle d_{\pm}|)U(\tau)]^{m-1}$ is parity symmetric, *i.e.*,

$$\mathcal{P}U(\tau)[(\mathbb{1} - |d_{\pm}\rangle \langle d_{\pm}|)U(\tau)]^{m-1}\mathcal{P} = U(\tau)[(\mathbb{1} - |d_{\pm}\rangle \langle d_{\pm}|)U(\tau)]^{m-1}. \quad (\text{SM12})$$

It then follows that

$$\langle d_+ | U(\tau) \left[\left(\mathbb{1} - |d_{\pm}\rangle \langle d_{\pm}| \right) U(\tau) \right]^{m-1} |d_-\rangle = 0, \quad (\text{SM13})$$

$$\langle d_- | U(\tau) \left[\left(\mathbb{1} - |d_{\pm}\rangle \langle d_{\pm}| \right) U(\tau) \right]^{m-1} |d_+\rangle = 0. \quad (\text{SM14})$$

Plugging them in Eq. (SM11), we finally obtain

$$\phi_{m+1}^{(L)} = \frac{1}{\sqrt{2}} \left[\chi_{m+1}^{(+)} + \chi_{m+1}^{(-)} \right]. \quad (\text{SM15})$$

This completes the induction and establishes the mapping (SM1) for arbitrary n . The derivation for the right boundary also follows in the same way.

II. EIGENVALUES OF THE SINGLE-TARGET SURVIVAL OPERATORS

In Eq. (SM11), we saw that the detection amplitudes $\chi_n^{(\pm)}$ are characterized by the survival operators

$$\mathcal{S}_{\pm} = \left(\mathbb{1} - |d_{\pm}\rangle \langle d_{\pm}| \right) U(\tau). \quad (\text{SM16})$$

The eigenspectrum of \mathcal{S}_{\pm} determines the behavior of $\chi_n^{(\pm)}$. Here, we examine their eigenvalues for the nearest-neighbor tight-binding Hamiltonian. These results are summarized in Table I, and we derive them below. For simplicity, we present the derivation for \mathcal{S}_- . The same steps can be carried out for \mathcal{S}_+ .

The eigenvalues and the eigenstates of the Hamiltonian are given by

$$E_k = -2 \cos \left(\frac{\pi k}{N+1} \right), \quad |E_k\rangle = \sqrt{\frac{2}{N+1}} \sum_{x=1}^N \sin \left(\frac{\pi k x}{N+1} \right) |x\rangle, \quad (\text{SM17})$$

where $k = 1, 2, \dots, N$. The target state $|d_-\rangle = (|1\rangle - |N\rangle)/\sqrt{2}$ becomes

$$|d_-\rangle = \frac{2}{\sqrt{N+1}} \sum_{\substack{k=1 \\ k \in \text{even}}}^N \sin \left(\frac{\pi k}{N+1} \right) |E_k\rangle. \quad (\text{SM18})$$

Let λ_- denote the eigenvalue of \mathcal{S}_- . It satisfies the characteristic equation

$$\det(\lambda_- \mathbb{1} - \mathcal{S}_-) = 0, \quad (\text{SM19})$$

$$\implies \det(\lambda_- \mathbb{1} - U(\tau) + |d_-\rangle \langle d_-| U(\tau)) = 0, \quad (\text{SM20})$$

$$\implies \det(\lambda_- \mathbb{1} - U(\tau)) \times \left(1 + \left\langle d_- \left| \frac{U(\tau)}{\lambda_- \mathbb{1} - U(\tau)} \right| d_- \right\rangle \right) = 0. \quad (\text{SM21})$$

Operator	Type	Eigenvalues	Count for even N	Count for odd N
\mathcal{S}_-	$ \lambda_- = 1$	$\{e^{-iE_k\tau}\}$ with k odd	$N/2$	$(N+1)/2$
\mathcal{S}_-	$ \lambda_- = 0$	0	1	1
\mathcal{S}_-	$0 < \lambda_- < 1$	$\sum_{k \in \text{even}} \frac{\sin^2(\omega_k)}{\lambda_- - e^{2i\tau \cos(\omega_k)}} = 0$	$N/2 - 1$	$(N-3)/2$
\mathcal{S}_+	$ \lambda_+ = 1$	$\{e^{-iE_k\tau}\}$ with k even	$N/2$	$(N-1)/2$
\mathcal{S}_+	$ \lambda_+ = 0$	0	1	1
\mathcal{S}_+	$0 < \lambda_+ < 1$	$\sum_{k \in \text{odd}} \frac{\sin^2(\omega_k)}{\lambda_+ - e^{2i\tau \cos(\omega_k)}} = 0$	$N/2 - 1$	$(N-1)/2$

TABLE I. Eigenvalues of the survival operators $\mathcal{S}_\pm = (\mathbb{1} - |d_\pm\rangle\langle d_\pm|)U(\tau)$ for the nearest-neighbor tight binding Hamiltonian.

In the last line, we have used the matrix determinant lemma: For an invertible square matrix A and column vectors $|u\rangle$ and $|v\rangle$

$$\det(A + |u\rangle\langle v|) = \det(A) \times (1 + \langle v|A^{-1}|u\rangle). \quad (\text{SM22})$$

Eq. (SM21) implies that

$$\det(\lambda_- \mathbb{1} - U(\tau)) = 0, \quad \text{or} \quad \left(1 + \left\langle d_- \left| \frac{U(\tau)}{\lambda_- \mathbb{1} - U(\tau)} \right| d_- \right\rangle\right) = 0. \quad (\text{SM23})$$

The first condition yields $\lambda_- = e^{-iE_k\tau}$, i.e., the eigenvalues of $U(\tau)$. From Eq. (SM16), we see that such a solution occurs only if the corresponding eigenmode of $U(\tau)$ is orthogonal to the $|d_-\rangle$. Eq. (SM18) tells us that $\langle E_k | d_- \rangle = 0$ if k is odd. This means that

$$\lambda_- = \{e^{-iE_k\tau}\}, \quad \text{where } k \text{ is odd.} \quad (\text{SM24})$$

These account for $N/2$ eigenvalues of \mathcal{S}_- when N is even, and $(N+1)/2$ eigenvalues when N is odd. The remaining eigenvalues follow from the second condition in Eq. (SM23)

$$\lambda_- \left\langle d_- \left| \frac{\mathbb{1}}{\lambda_- \mathbb{1} - U(\tau)} \right| d_- \right\rangle = 0. \quad (\text{SM25})$$

The trivial solution is

$$\lambda_- = 0. \quad (\text{SM26})$$

Other solutions are

$$\left\langle d_- \left| \frac{\mathbb{1}}{\lambda_- \mathbb{1} - U(\tau)} \right| d_- \right\rangle = 0, \implies \sum_{\substack{k=1 \\ k \in \text{even}}}^N \frac{\sin^2(\omega_k)}{(\lambda_- - e^{2i\tau \cos(\omega_k)})} = 0, \quad (\text{SM27})$$

where $\omega_k = \pi k / (N+1)$. Eq. (SM27) can be interpreted in the language of the classical charge theory [47, 52]. The points $e^{2i\tau \cos(\omega_k)}$ (for even k) lie on the unit circle and act as sources with positive weights $\sin^2(\omega_k)$, while Eq. (SM27) is precisely the requirement that the net force field vanishes at λ_- , i.e., λ_- is an equilibrium point of the forces generated by these charges. Solving Eq. (SM27) generates the $(N/2 - 1)$ eigenvalues of \mathcal{S}_- for even N and $(N-3)/2$ for odd N located in the unit disc ($|\lambda_-| < 1$).

To sum up, Eqs. (SM24, SM26, SM27) give the N eigenvalues of the \mathcal{S}_- operator. These results are summarized in Table I, which also lists the eigenvalues of \mathcal{S}_+ .

III. RELATION OF THE SPLITTING PROBABILITY WITH THE EIGENVALUES OF THE SURVIVAL OPERATOR

In the Letter, we pointed out that the interference term $\xi(x_0, N, \tau)$ can be written as an expansion in the eigenvalues of the \mathcal{S}_- survival operator. Here, we derive this expansion. Recall that the splitting probabilities are given by

$$P_L(x_0) = \frac{1}{2} + \xi(x_0, N, \tau), \quad P_R(x_0) = \frac{1}{2} - \xi(x_0, N, \tau), \quad (\text{SM28})$$

where the term $\xi(x_0, N, \tau)$ is

$$\xi(x_0, N, \tau) = \operatorname{Re} \left[\oint_{|z|=1} dz \mathcal{I}(z, x_0, N, \tau) \right], \quad \text{with} \quad (\text{SM29})$$

$$\mathcal{I}(z, x_0, N, \tau) = \frac{1}{2\pi iz} \left[\frac{\sum_{k \in \text{even}} \sin(\omega_k) \sin(\omega_k x_0) \left(\frac{e^{-2i\tau \cos(\omega_k)}}{z - e^{-2i\tau \cos(\omega_k)}} \right)}{\sum_{k \in \text{even}} \sin^2(\omega_k) \left(\frac{1}{z - e^{-2i\tau \cos(\omega_k)}} \right)} \right] \left[\frac{\sum_{k \in \text{odd}} \sin(\omega_k) \sin(\omega_k x_0) \left(\frac{e^{2i\tau \cos(\omega_k)}}{1-z e^{2i\tau \cos(\omega_k)}} \right)}{\sum_{k \in \text{odd}} \sin^2(\omega_k) \left(\frac{1}{1-z e^{2i\tau \cos(\omega_k)}} \right)} \right], \quad (\text{SM30})$$

where $\omega_k = \pi k/(N+1)$. Eq. (SM29) indicates the contour integration of a complex function $\mathcal{I}(z, x_0, N, \tau)$ over a unit circle. By the residue theorem, this integral can be evaluated as the sum of the residues of $\mathcal{I}(z, x_0, N, \tau)$ at its singularities inside the contour. Let us analyze its singularities.

A numerical inspection of Eq. (SM30) reveals that the only singularities present are simple poles. The first pole is $z_{\text{pole}} = 0$. Other poles are obtained by solving

$$\sum_{k \in \text{even}} \sin^2(\omega_k) \left(\frac{1}{z_{\text{pole}} - e^{-2i\tau \cos(\omega_k)}} \right) = 0, \quad (\text{SM31})$$

$$\sum_{k \in \text{odd}} \sin^2(\omega_k) \left(\frac{1}{1 - z_{\text{pole}} e^{2i\tau \cos(\omega_k)}} \right) = 0. \quad (\text{SM32})$$

Comparing Eq. (SM31) with the eigenvalue condition for \mathcal{S}_- in Table I, we identify $z_{\text{pole}} = \lambda_-^*$ (where $*$ denotes complex conjugation). In particular, Eq. (SM31) corresponds to the nontrivial eigenvalues of \mathcal{S}_- , which satisfy $0 < |\lambda_-| < 1$. Hence $0 < |z_{\text{pole}}| < 1$, so these poles lie inside the unit disk and contribute to the contour integral in Eq. (SM29).

Similarly, comparing Eq. (SM32) with Table I, we find that these poles are related to the eigenvalues of \mathcal{S}_+ via $z_{\text{pole}} = 1/\lambda_+$. Since Eq. (SM32) corresponds to the nontrivial eigenvalues of \mathcal{S}_+ , which satisfy $0 < |\lambda_+| < 1$, it follows that $|z_{\text{pole}}| = |1/\lambda_+| > 1$. Hence these poles lie outside the unit disc and do not contribute to the contour integral in Eq. (SM29).

Therefore, $\xi(x_0, N, \tau)$ is determined solely by the poles $z_{\text{pole}} = \lambda_-^*$ corresponding to the eigenvalues of \mathcal{S}_- with $|\lambda_-| < 1$ (including $\lambda_- = 0$)

$$\xi(x_0, N, \tau) = -2\pi \sum_{|\lambda_-| < 1} \operatorname{Im} [\operatorname{Residue}[\mathcal{I}; z = \lambda_-^*]], \quad (\text{SM33})$$

where $\operatorname{Residue}[\mathcal{I}; z = \lambda_-^*]$ denotes the residue of the function $\mathcal{I}(z, x_0, N, \tau)$ at the pole $z = \lambda_-^*$. This relation makes explicit that $\xi(x_0, N, \tau)$ can be written as a summed contribution of the eigenvalues $\{\lambda_-\}$.

IV. SPECTRAL ORIGIN OF THE TRANSITION IN THE SPLITTING PROBABILITY

In the Letter, we demonstrated that for $N \gg 1$, the splitting probabilities exhibit a transition at a critical sampling time $\tau_c = \pi/2$. For $\tau \leq \tau_c$, both $P_L(x_0)$ and $P_R(x_0)$ are equal to 1/2, independent of x_0 and τ . Above criticality, for $\tau > \tau_c$, they instead depend on x_0 and τ . As was pointed out in the Letter, this behavior originates from a qualitative change in the arrangement of the eigenvalues $\{\lambda_-\}$ of the operator \mathcal{S}_- , which, according to Eq. (SM33), induces a change in the interference term $\xi(x_0, N, \tau)$ and hence the splitting probabilities via Eq. (SM28).

In panels (a-e) of Fig. 5, we employ Eq. (SM27) (also see Table I) to numerically obtain the eigenvalues $\{\lambda_-\}$ for five different sampling times, (a) $\tau = 1$, (b) $\tau = \pi/2$, (c) $\tau = 2$, (d) $\tau = 3.75$, and (e) $\tau = 6$. The system size is kept fixed to $N = 61$. Panel (a) corresponds to $\tau < \tau_c$, panel (b) to $\tau = \tau_c$, and panels (c-e) to $\tau > \tau_c$. For $\tau = 1$, we see in (a) that all eigenvalues, except the one at the origin, lie close to the unit circle and are distributed regularly along a single arc between the points $a_1(\tau)$ and $a_2(\tau)$ (shown in red in (a)). By numerical inspection, we find $a_1(\tau) = \exp(-iE_{\max}\tau)$ and $a_2(\tau) = \exp(-iE_{\min}\tau)$, where $E_{\max} \approx 2$ and $E_{\min} \approx -2$ are the maximum and minimum energies for large system sizes. For such a regular arrangement of $\{\lambda_-\}$, the contributions associated with different eigenvalues in Eq. (SM33) exhibit strong cancellations, resulting in a negligible $\xi(x_0, N, \tau)$. For example, with $x_0 = 11$ and $N = 61$, we obtain $\xi(x_0, N, \tau = 1) \approx 0.002$. Plugging this result in Eq. (SM28) then gives $P_L(x_0) \approx P_R(x_0) \approx 1/2$.

As we increase τ , the eigenvalues remain still close to the unit circle, distributed regularly along a single arc between the points $a_1(\tau)$ and $a_2(\tau)$. However, as τ approaches the critical point

$$\tau_c = 2\pi/\Delta E \quad (\text{SM34})$$

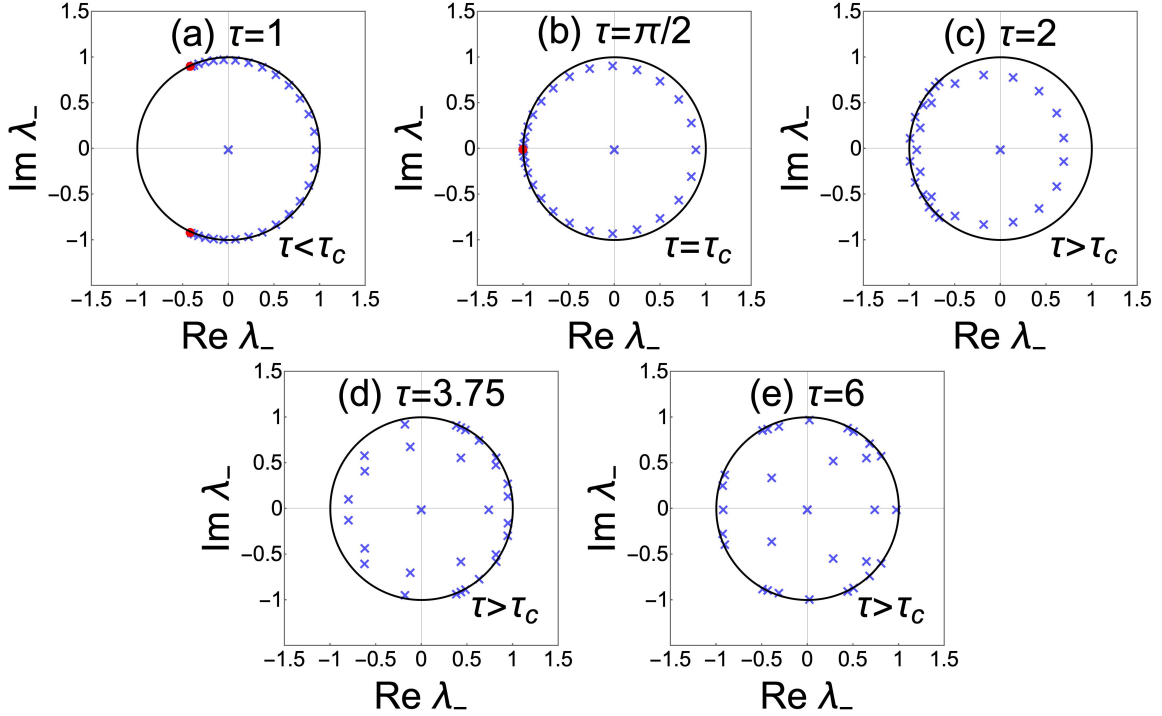


FIG. 5. Eigenvalues $\{\lambda_-\}$ (where $|\lambda_-| < 1$) of the survival operator $\mathcal{S}_- = (1 - |d_- \rangle \langle d_-|) U(\tau)$ for the nearest-neighbor tight-binding Hamiltonian. They are obtained by solving Eq. (SM27) numerically (also see Table I). Panels (a-e) show these eigenvalues for five different sampling times with $N = 61$. For $\tau \leq \tau_c$, they are distributed along a single arc between the points $a_1(\tau) = e^{-iE_{\max}\tau}$ and $a_2(\tau) = e^{-iE_{\min}\tau}$ [shown in red in (a-b)] where $E_{\max} \approx 2$ and $E_{\min} \approx -2$ are the maximal and minimal energy eigenvalues for $N \gg 1$. For $\tau > \tau_c$, there is a qualitative change in the eigenvalue arrangement. The single arc breaks into distinct branches in the unit disk, and the arrangement becomes somewhat irregular. This, in turn, leads to qualitative change in $\xi(x_0, N, \tau)$ in Eq. (SM33). For $x_0 = 11$, $N = 61$, we find (a) $\xi(x_0, N, \tau) = 0.002$ for $\tau = 1$, (b) $\xi(x_0, N, \tau) = -0.002$ for $\tau = \tau_c$, (c) $\xi(x_0, N, \tau) = -0.03$ for $\tau = 2$, (d) $\xi(x_0, N, \tau) = -0.135$ for $\tau = 3.75$ and (e) $\xi(x_0, N, \tau) = 0.132$ for $\tau = 6$. Plugging these results in Eq. (SM28), we obtain $P_L(x_0) \approx P_R(x_0) \approx 1/2$ for $\tau \leq \tau_c$ and $P_L(x_0) \neq P_R(x_0) \neq 1/2$ for $\tau > \tau_c$.

where $\Delta E = (E_{\max} - E_{\min})$, the two points coalesce on the negative real axis, i.e., $a_1(\tau) = a_2(\tau) = -1$, and the arc closes; see the red points in (b). Here again, the term $\xi(x_0, N, \tau)$ in Eq. (SM33) is small. For same values of x_0 and N , we find $\xi(x_0, N, \tau = \pi/2) \approx -0.002$, leading to $P_L(x_0) \approx P_R(x_0) \approx 1/2$.

Beyond this critical point, the situation changes qualitatively. The points $a_1(\tau)$ and $a_2(\tau)$ move past each other on the unit circle. Here, we find that the arrangement of the $\{\lambda_-\}$ changes and is no longer restricted to a single arc, see (c-e). Instead, the distribution becomes irregular, with eigenvalues spreading nonuniformly inside the unit disk. Here, the contributions of different eigenvalues in Eq. (SM33) no longer cancel as efficiently, and $\xi(x_0, N, \tau)$ becomes appreciable for $\tau > \tau_c$. For example, for $x_0 = 11$ and $N = 61$, we obtain $\xi(x_0, N, \tau = 2) \approx -0.03$, $\xi(x_0, N, \tau = 3.75) \approx -0.135$, and $\xi(x_0, N, \tau = 6) \approx 0.132$. Thus, the term $\xi(x_0, N, \tau)$ is not generally negligible for $\tau > \tau_c$. This leads to deviations from 1/2 for $\tau > \tau_c$ for the splitting probabilities via Eq. (SM28).

To summarize, as τ is tuned across τ_c , the eigenvalues $\{\lambda_-\}$ arrangement undergoes a qualitative change, which directly alters the residue sum in Eq. (SM33) and thereby leads to the transition in the splitting probabilities in Eq. (SM28).